Collective amplification of nearby nanoparticles in the Coulomb blockade restricted charging of a single nanoparticle

Baptiste Chatelain, Ali El Barraj, Clémence Badie, Lionel Santinacci, Clemens Barth

Collective amplification of nearby nanoparticles in the Coulomb blockade restricted charging of a single nanoparticle

Baptiste Chatelain, Ali El Barraj, Clémence Badie, Lionel Santinacci and Clemens Barth

[2]Aix-Marseille Univ, CNRS, CINaM, Marseille, France

Abstract. The characterization of charges in oxide supported metal nanoparticles (NP) is of high interest in research fields like heterogeneous catalysis and microelectronics. A general desire is to manipulate the charge of an oxide supported single NP and to characterize afterwards the charge and its interference with the insulating support but also with nearby NPs in the vicinity. By using noncontact AFM (nc-AFM) and Kelvin probe force microscopy (KPFM) in ultra-high vacuum (UHV) and at room temperature we show that a ∼5 nm small AuNP can be directly charged with electrons by the AFM tip and that upon the charging, nearby AuNPs sensitively change their electrostatic potential with a large impact on the charge detection by nc-AFM and KPFM. The AuNPs are supported on a 40 nm thick insulating Al_2O_3 film, which is grown by atomic layer deposition (ALD) on Si(001). Due to Coulomb blockades, the NP charging appears in the form of large and discrete peaks in detuning versus bias voltage curves. Finite element method (FEM) calculations reveal that the large peaks can only be observed when the potentials of nearby insulated NPs get modified by the NP's electron charge, according to the electrostatic induction principle. In view of the number of transferred electrons, we anticipate that after the charging, the electrons are transferred from the AuNP to the NP-Al_2O_3 interface or into Al_2O_3 subsurface regions directly underneath.

[♯]Corresponding author: barth@cinam.univ-mrs.fr

1. Introduction

Charges on oxide supported metal nanoparticles (NP) are of high interest in heterogeneous catalysis and microelectronics due to their impact onto the NP's electronic properties and their interference with defects of the underlying support and with other NPs in close vicinity. Whereas the first aspect is of importance in catalysis, the second one is of particular interest in microelectronics because a detailed analysis of the charge-insulator interaction but also the charge interaction with other nearby nano-objects can explain phenomena that are related to leakage currents and device characteristics and performance.

A general desire is to manipulate the charge of a single nano-object and to characterize the manipulated charge and its interaction with its environment afterwards, which can be best accomplished with atomic force microscopy (AFM) [1], as recently demonstrated at a single carbon nanotube [2], molecular island [3], single molecule [4, 5], single atom [6] and also at a single NP [7, 8, 9, 10, 11, 12]. A charge manipulation experiment starts with transferring the charge by applying a bias voltage between the AFM tip and surface, with the tip being placed at some nanometre distance above the surface. Afterwards in a second step, the surface is either imaged or studied by spectroscopy, which both reveal changes of the surface potential that are due to the injected charges.

Thanks to noncontact AFM (nc-AFM), the AFM tip can be placed at any distance with sub-nanometre precision above the NP so that charges can be injected in a controlled way and without contacting the tip with the NP. This is mostly done by single-point spectroscopy, where the tip-NP interaction is recorded during a sweep of the bias voltage [7, 4, 12]. The advantage of single-pass Kelvin probe force microscopy (KPFM) is the high spacial resolution as well as the high resolution in the surface potential that can be obtained at NPs, in particular, if experiments are accomplished under ultra-high vacuum (UHV) conditions [13, 14, 15, 16, 17, 18, 19].

In recent years, single electron phenomena related to Coulomb blockades have been characterized at NPs by spectroscopy [7, 8, 10] or by dissipation nc-AFM imaging under UHV conditions [9, 11]. For such manipulation experiments, the NP is placed on a thin insulating film which the latter is supported on a conducting support. The bias voltage is chosen such that electrons are exchanged between the conducting support and the NP by passing through the thin insulating film. In spectroscopy, the parabolic shape of the tip-surface interaction exhibits characteristics jumps that can be assigned to a single electron transfer [7, 8, 10] whereas in dissipation images an electron transfer is visible in the form of a characteristic sharp and concentric ring around the NP [9, 11]. However, a requisite for such charge manipulation experiments is that the insulating film has to be relatively thin such that tunnelling of charges between the support and the NP is guaranteed. This excludes experiments on thick insulating films and bulk insulators. Furthermore, the interaction between the charged NP and NPs in close vicinity has not been considered so much.

Here we show that by using nc-AFM spectroscopy and KPFM in UHV and at room temperature (RT), Coulomb blockades can nevertheless be observed at an insulator supported single metal NP if the NP is charged by the AFM tip. Similar tip-charging experiments were carried out at a molecular island [3], single molecule [4] and at a very large NP [12] but, so far, not at a metal NP, which has a size of a few nanometres only. We demonstrate the Coulomb blockade restricted charging with AuNPs, which are supported on thick insulating, atomic layer deposition (ALD)

grown Al_2O_3 films. Charge trapping in such armorphous films is an important topic in research since these films are used as a passivation material for solar cells [20, 21] and as an interface layer in flash memory devices [22, 23]. We use finite element method (FEM) calculations to explain fundamental electrostatic phenomena in the charge detection and explicitly show that a collective amplification of nearby NPs based on the electrostatic induction principle sensitively influences the charge detection. Furthermore, we discuss that a possible charge exchange between the charged NP and the Al_2O_3 support takes place.

2. Methods

A detailed description of the sample preparation, STM, nc-AFM, KPFM and FEM as well as additional experiments and FEM calculations can be found in the supplementary information. Here, we summarize the most important details.

2.1. Alumina films and NPs

Amorphous Al_2O_3 films with a thickness of 15 and 40 nm are grown by atomic layer deposition on Si(001) substrates kept at 200 °C, following a procedure described earlier [24, 25]. For the growth, trimethylaluminium (TMA, 98 %) and ultra-pure water are used. Immediately after the film growth, the Al_2O_3 samples are transferred into a UHV chamber, in which they are annealed either in UHV or in 5×10^{-6} mbar O_2 between 500 and 650 °C. Nanometre sized AuNPs are then grown in UHV by evaporating neutral atoms onto an Al_2O_3 film, which is kept at a temperature between 500 and 650 °C.

2.2. Scanning probe microscopy

Frequency modulated nc-AFM and single-pass frequency modulated KPFM experiments are performed in ultra-high vacuum (1×10^{-10} mbar base pressure) [26] with a room temperature AFM/STM. During the scanning of the surface, the electrostatic tip-surface interaction is minimized at each image point of the surface by the bias voltage U_{Bias}, which is applied at the backside of the sample (tip at ground). The minimizing so-called Kelvin voltage contains the contact potential difference between the tip and the conducting support under the influence of the dielectric Al_2O_3 film but also a contribution of all charges on and in the film [27, 28]. To simplify, we refer to the *Kelvin voltage* and to the corresponding *Kelvin images*. A Kelvin image is simultaneously obtained with the topography nc-AFM image. A dark blue (green/orange) contrast corresponds to less (more) positive Kelvin voltages.

2.3. FEM calculations

Calculations are done with with the Open Source platform FEniCS [29], which solves the Poisson equation and calculates the electrostatic potential between all objects (AFM tip, NPs, dielectric film and conducting support) and in turn the tip-surface force and the potentials of the NPs. For the modelling of the objects, a three-dimensional (3D) mesh model is built with help of the Open Source program Gmsh [30]. A self-written Python program coordinates the creation of the 3D mesh and following FEniCS calculations.

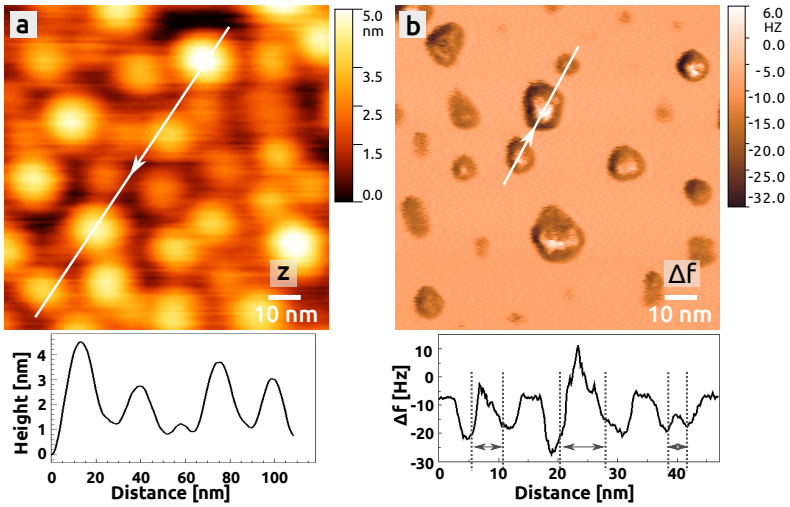

Figure 1. Topography (a) and detuning △f image (b) of a 40 nm thick Al_2O_3 film with supported AuNPs. NP growth: 4.3 ML Au at 500 °C, nc-AFM: $\triangle f$ = -6.0 (a) and -8.9 Hz (b), f_0 = 72.4 (a) and 317.4 kHz (b), v = 0.5 (a) and 9.8 Hz (b), KPFM (a): U_{ac} = 300 mV, f_{ac} = 620 Hz.

3. Results

3.1. Tip induced NP-Al_2O_3 charging

Figure 1 shows typical supported AuNPs grown at 500°C on a 40 nm thick Al_2O_3 film, which the latter has a surface roughness well below 1 nm (see figure S1 in the supplementary material). Due to the amorphous structure of the Al_2O_3 film, a high NP density of $\varrho_{Au} = 3.0 \times 10^{11}$ NP/cm^2 is found. The AuNPs have a mean height of $h_{Au} = (3.9 \pm 0.3)$ nm and an apparent lateral size of $d_{Au} = (15.9 \pm 0.7)$ nm in the topography image (figure 1(a) and figure S2 in the supplementary material). Because of the tip-surface convolution effect, the lateral size is too large and constant height mode imaging [31] yields a more credible value between 5 and 10 nm (see vertical lines in figure 1(b)).

In general, imaging the AuNP/Al_2O_3 surface occasionally leads to instabilities of the tip-surface interaction and in turn to tip changes, which accidentally occur (see horizontal lines in figure 2(a) and (b)). In a few cases, the tip may remove some NPs from the surface, as it has been the case in the upper part of both images in figure 2 (position 1). In this region, only the Al_2O_3 film surface is visible, which is about 4.5 nm lower in height than the NPs. The NPs exhibit a brighter contrast than Al_2O_3 in the corresponding Kelvin image, which corresponds to potential difference of -0.6 V between the Al_2O_3 film and the AuNPs (figure 2(c)). A brighter contrast corresponds to a more negative surface potential [32], and assuming that the Al_2O_3 is neutral, it can be concluded that the AuNPs are more negative than the Al_2O_3 film. We anticipate that a possible intrinsic charge transfer from Al_2O_3 to the NPs is responsible for this.

A regular observation is that after having scanned a small surface region by KPFM, a following scan with a larger image size shows the previously scanned region in a different Kelvin contrast: in the middle of the image in figure 2(b), a rectangle

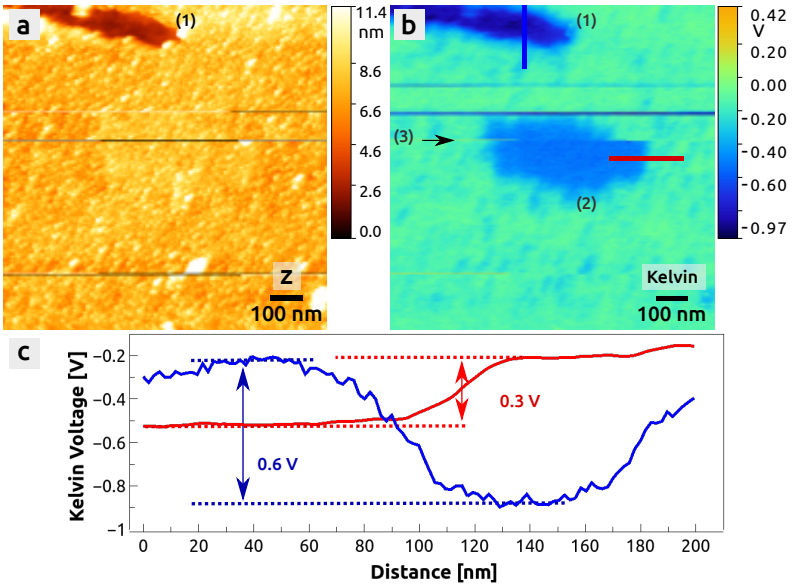

Figure 2. Tip induced charging between AuNPs and a 15 nm thick Al_2O_3 film. (a) and (b) Topography (a) and corresponding Kelvin image (b) with two profiles (c) presenting typical Kelvin voltages at the position of the colour coded lines in the Kelvin image (b). Due to a tip retraction that happens upon a tip-change at position (3), the previously scanned square region is distorted to a rectangle. AuNP growth: 3.1 ML at 650 °C, nc-AFM: $\triangle f$ = -6.55 Hz, f_0 = 70.88 kHz, v = 0.5 Hz, KPFM: U_{ac} = 300 mV, f_{ac} = 620 Hz.

with a light blue contrast corresponding to a -0.3 V strong potential drop can be seen (position 2). The horizontal length of the rectangle equals the size of the quadratic region previously scanned (figure S4 in the supplementary material). When imaging such a surface area during an hour, the region gets larger and distorted by time until the entire scanned region exhibits the same low surface potential (figure S4 in the supplementary material). All this shows that the surface potential gets obviously modified by the AFM tip, even in the KPFM mode where the electrostatic tip-surface interaction is minimized during the scanning. Although a polarization effect of the AuNP/Al_2O_3 system cannot be excluded, it seems more likely that the tip induces an exchange of electrons from the NPs back to the Al_2O_3 film.

3.2. Uncontrolled tip-charging of AuNPs

For charge manipulation experiments at a single NP, spectroscopy as described in, e.g., references [7, 12] can be used: a NP is selected during the scanning and a detuning versus bias voltage spectroscopy curve [$\triangle f(U_{Bias})$] is then recorded above the selected NP (no scanning) at either a reduced [12] or increased [7] tip-surface distance, or at the distance used for the scanning before (see drawing 1 in figure 3(a)). In our experiments, a decrease of the distance by even a few Ångström always leads to instabilities in the tip-surface interaction because the tip, being generally already close to the surface, gets into contact with the NPs. When taking $\triangle f(U_{Bias})$ curves at the distance of the imaging, spectroscopy is more stable and $\triangle f(U_{Bias})$ curves can be obtained.

In the curve of figure 3(b) (inset), the forward (red) and backward sweep (blue)

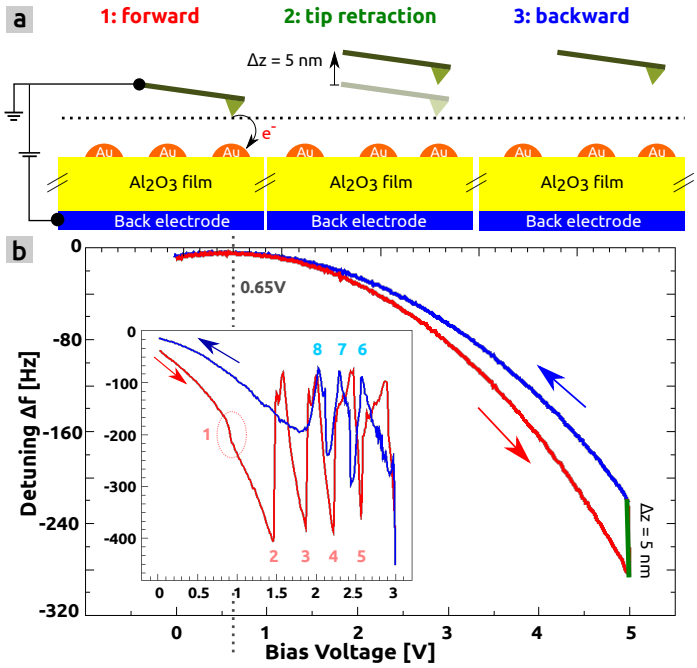

Figure 3. (a) The position of the tip during a spectroscopy step for controlled charge manipulation experiments. (b) Experimental $\triangle f(U_{\mathrm{Bias}})$ spectroscopy curves obtained above a 40 nm Al_2O_3 film with AuNPs (large graph) and above a selected AuNP grown on a 15 nm film (inset). Spectroscopy: $n_{\mathrm{points}} = 500$, $\tau = 5.12$ ms, $\nu_{\mathrm{Bias}} = 4.64$ V/sec, $t = 2.59$ sec, $\triangle z = +5.0$ nm (not inset), $f_0 = 70.88$ kHz.

of a $\triangle f(U_{\mathrm{Bias}})$ curve are shown, obtained at an unchanged distance above a single NP. At the beginning of the forward sweep, the characteristic parabolic shape of the $\triangle f(U_{\mathrm{Bias}})$ curve is visible. However, at a voltage of +0.90 V, the detuning suddenly decrease vertically by -40 Hz (1) and continues afterwards its parabolic shape, until a voltage of +1.46 V (2). At this voltage and at other three voltages (+1.87 V (3), +2.22 V (4) and +2.57 V (5)) characteristics strong peaks of the detuning appear, where the detuning instantaneously increases by roughly +300 Hz. Three similar peaks can be observed also during the backward sweep (blue) at +2.5 V (6), +2.2 V (7) and +2.0 V (8).

Further below it will be explained that the sudden changes in the detuning $\triangle f$ are due to a transfer of a few electrons between the tip and the NP. If after the spectroscopy the surface region is scanned on a slightly larger scale by KPFM, generally no NP can be found that carries a charge as explained below (see figure S4 in the supplementary material). We speculate that in such cases, charges are transferred from the tip to the NP during the forward sweep but that they are then extracted from the NP to the tip during the backward sweep with the result that effectively no net charge is transferred to the NP. Apart from experiments like those ones shown in figure 3(b) (inset), controlled charge manipulation experiments remain generally challenging if the back-transfer of charges is not inhibited.

3.3. Controlled tip-charging of AuNPs

To better control the charging of a NP, the principle in figure 3(a) is used. The tip-surface distance, which is determined by the pre-set value of the detuning $\triangle f$ during the imaging before, is used for the forward sweep (1). In this case the tip is relatively close to the NP such that charging events can occur. However, to avoid the probability of a back-transfer of charges to the tip, the tip-surface distance is increased by some nanometres (e.g., by $\triangle z = +5\,\mathrm{nm}$) at the end of the forward sweep (2). At this increased distance, the backward sweep is recorded where the typical parabolic shape of the $\triangle f(U_{\mathrm{Bias}})$ curve is obtained. The experimental $\triangle f(U_{\mathrm{Bias}})$ curve in figure 3(b) (large graph) shows the typical shape of the two parabolic curves obtained above a AuNP/Al_2O_3(15 nm) surface in a secured large tip-surface distance (charging inhibited). Note that because the tip-surface distance is increased during the backward sweep, the parabola is wider than the one during the forward sweep due to the decreased tip-surface capacitance. Note also that the maxima of both curves are at the exact same bias voltages ($U_{\mathrm{Bias},0} = 0.65\,\mathrm{V}$) and detuning values because there has been no charging event.

Figure 4 shows typical controlled charge manipulation experiments at single AuNPs. Before the charging, the Kelvin image (figure 4(b)) shows a rather homogeneous surface potential with a mean value of $U_{\mathrm{Kelvin,before}} = +0.09\,\mathrm{V}$ and variations of up to 0.3 V, which cannot be precisely related to the distribution of the NPs. We stress here that this strongly depends on the size of the tip apex since we sometimes observe a strong, well-defined Kelvin contrast at single NPs with, e.g., other tips or after a tip-change. In the case here, the tip apex is obviously blunt such that the large tip apex integrates the long-range electrostatic tip-surface interaction over a large ensemble of NPs at each point of the surface (tip-surface convolution). In contrast, the interaction is more confined in the tip-surface interaction that determines the topography image, due to the short-range character of the involved forces. We assume that the tip has a nanotip at the apex that leads to the relatively sharp NP contrast in the topography image (figure 4(a)).

Figure 4(c) and (d) shows a typical charging experiment: during the imaging, eight NPs are selected (see labels in figure 4(a)) above which the type of spectroscopy from figure 3(a) is conducted, with a tip retraction distance of +5.0 nm after the forward sweep. Because of the creep of the x, y, z scanner, the tip does not image the exact same surface position when the scanning is resumed after a spectroscopy measurement has been done. This leads to slight shifts of the image contrast and to horizontal bright/dark streaks. Note that a spectroscopy measurement is generally executed at a selected NP which has been imaged just before by the tip (scanning from bottom to the top). The result is that after a spectroscopy measurement has been conducted (at the bright/dark streaks), a strong contrast change can sometimes be seen directly above the respective NP, in the following scanning lines of the Kelvin but also topography image. This is the case for the NPs 1, 4, 6 and 8, which got indeed charged as explained below. Note that the charging depends strongly on the tip-NP distance. Because a precise positioning of the tip above a selected NP is already at the limit with our AFM, the tip-NP distance has been obviously a bit too large for NPs 2, 3, 5 and 7, which could not have been charged.

The KPFM experiment in figure 4(e) and (f) shows the same surface region after the eight charge manipulation experiments. The Kelvin image shows a very strong contrast change of the surface potential in comparison to the initial situation

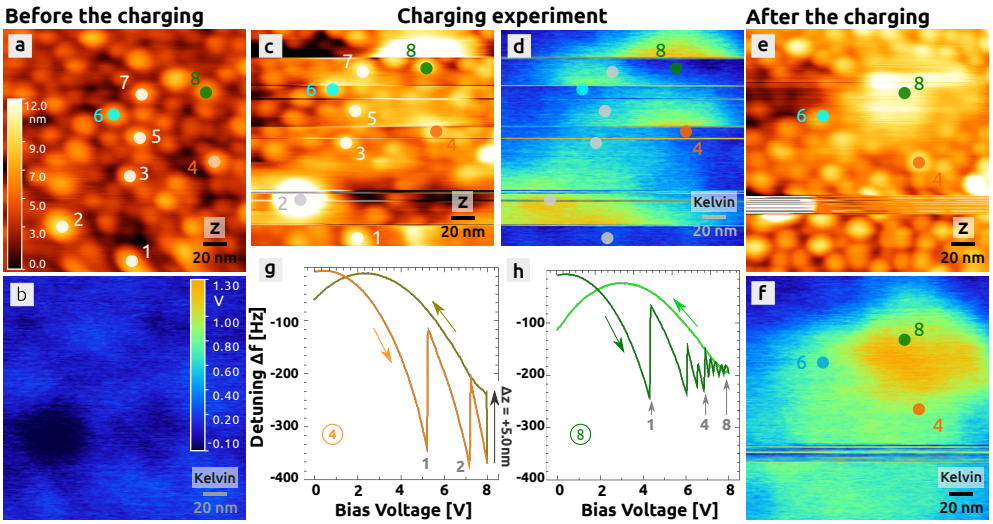

Figure 4. Charging single AuNPs on a 40 nm thick Al_2O_3 film. All Kelvin images ((b), (d) and (f)) have the same colour scale as well as the topography images ((a), (c) and (e)). AuNP growth: 3.7 ML Au at 650 °C, KPFM: $\triangle f$ = -7.0 Hz ((a) - (d)) and -7.76 Hz ((e) and (f)), all: f_0 = 70.88 kHz, v = 0.5 Hz, U_{ac} = 500 mV, f_{ac} = 620 Hz. Spectroscopy: n_{points} = 500, τ = 10.24 ms, ν_{Bias} = 3.11 V/s, t = 5.15 s, $\triangle z$ = +5.0 nm.

(figure 4(b)), with a maximum Kelvin voltage of $U_{Kelvin,after} = +1.3$ V. The surface potential has therefore increased by $\triangle U_{Kelvin} = +1.2$ V. According to the contrast formation of charges on insulators [33, 32], it can be concluded that negative charges (electrons) have been transferred from the tip into the NPs because the Kelvin voltage increases towards more positive values. The injected charge remains on a time scale of hours, as shown by figure S5 in the supplementary material. Important to note is that the maximum Kelvin contrast can be roughly found in the triangle formed by NP 4, 6 and 8, which could be indeed charged (see below). Furthermore, the electrostatic tip-surface interaction is obviously so strong that the residual Coulomb force between tip and surface, which cannot be compensated by KPFM, leads to a strong change also in the topography image between NPs 4, 6 and 8. Note that in both images, the increased contrast covers several NPs and that no sharp NP specific contrast can be seen, which is due to the above mentioned convolution effect of the tip apex.

From the eight selected NPs, only four could be charged during the series of spectroscopy experiments as follows: NP 2, 3, 5 and 7 remain uncharged because the forward and backward $\triangle f(U_{Bias})$ curves (not shown) do not exhibit any signatures of a charge transfer but rather the perfect course of the parabola, similar to the curve shown in figure 3(b) (large graph). Accordingly, the topography and Kelvin images in figure 4(c) and (d) do not show any remarkable enhanced contrast above the NPs. However, NPs 1, 4, 6 and 8 show signatures of charging events as it will be discussed in the following, with the curves in figure 4(g) and (h) for NP 4 and 8.

The forward $\triangle f(U_{Bias})$ curve shows first the typical parabolic course of the detuning $\triangle f$ at relatively low bias voltages. Starting at elevated bias voltages, two (at +5.2 and +7.2 V) and eight large peaks (at +4.3, +6.1, +6.5, +6.9, +7.1, +7.3, +7.6 and +7.8 V) can be seen for NP 4 and 8, respectively. In contrast to the forward sweep,

the backward sweep does not show any charging events thanks to the increased tip-surface distance of $\triangle z = +5.0\,\mathrm{nm}$. In agreement with the Kelvin image in figure 4(f), which shows a more positive mean surface potential, both backward curves for NP 4 and 8 are displaced towards more positive bias voltages, which is a clear signature that electrons got transferred from the tip into the respective NP.

An interesting observation can be made: (a) the first two peaks of NP 4 appear at similar high voltages as the first two peaks of NP 8 (+5.2 and +7.2 V versus +4.3 and +6.1 V). Secondly, the next-neighbour voltage differences of NP 8 starts with a relatively large value of 1.8 V, and decreases onto an almost equidistant difference of 0.3 V afterwards ($\triangle U = 1.8$, 0.4, 0.4, 0.2, 0.2, 0.3, 0.2 V). Alongside, the peak height decreases from a high value of 174 Hz onto values of around 20 Hz (NP 8: 174, 94, 40, 76, 36, 20, 20, 18 HZ). The height of the two peaks at NP 4 are larger (NP 4: 231, 176 HZ).

The spectroscopy curve in figure 4(g) is again shown in figure 5(a) for a more detailed analysis. As it can be clearly seen, the course of the $\triangle f(U_{\mathrm{Bias}})$ curve in the forward sweep is still parabolic after the first and second peak at $U'_{\mathrm{Peak1}} = +5.2$ and $U'_{\mathrm{Peak2}} = +7.2\,\mathrm{V}$, respectively. The maxima have shifted towards more positive bias voltages, which means that the two branches lie on two different parabolas compared to the initial parabola covering the low voltage part. This is a clear signature that at a peak, electrons are transferred instantaneously within a very short time from the tip into the respective NP and that no charging event occurs on the three parabolic branches. The charging observed in all of our experiments is therefore discrete, appearing at specific voltages.

For a rough estimation of charges involved in the NP charging, the force model proposed in Ref. [7] can be considered:

$$F = \frac{1}{2}\,\frac{\partial C_{\mathrm{series}}}{\partial z}\,\left(U_{\mathrm{Bias}} - \frac{n\,e}{C_{\mathrm{sub}}}\right)^2 \tag{1}$$

The model includes the number of charges (n), electron charge (e) and the capacitance C_{series}, which is composed by the tip-NP (C_{tip}) and substrate-NP capacity (C_{sub}) and which is given by $C_{\mathrm{series}} = C_{\mathrm{tip}}\,C_{\mathrm{sub}}/(C_{\mathrm{tip}} + C_{\mathrm{sub}})$. Supposing that the detuning $\triangle f$ is proportional to the square of the voltage difference in equation (1), the simple equation $\triangle f(U_{\mathrm{Bias}}) = a\,(U_{\mathrm{Bias}} - U_{\mathrm{max}})^2$ with

$$U_{\mathrm{max}} = \frac{n\,e}{C_{\mathrm{sub}}} \tag{2}$$

can be used for the fitting. For the initial parabola in the low voltage range and for the parabola on the backward sweep, a maximum of $U_{\mathrm{ini}} = (0.74 \pm 0.02)\,\mathrm{V}$ (orange curve) and $U_{\mathrm{end}} = (2.37 \pm 0.02)\,\mathrm{V}$ (dark orange curve), respectively, are obtained. The other two parabola have their $\triangle f$ maxima clearly at more positive voltages: $U_1 = (2.86 \pm 0.02)\,\mathrm{V}$, $U_2 = (4.72 \pm 0.02)\,\mathrm{V}$. Note that for the fitting of the parabolic branches, we have included the offset value of $\triangle f_{\mathrm{max}} = $-7.0 Hz of the first parabola at low voltages, which we consider to be present also for all the other curves.

From the two maxima, U_1 and U_2, the ratio of charges$n_2\,/\,n_1$ can be obtained from equation (2):

$$n_2\,/\,n_1 \;=\; \frac{U_2 - U_{\mathrm{ini}}}{U_1 - U_{\mathrm{ini}}} \tag{3}$$

Here, we only consider the relative distance of the two voltages from the maximum U_{ini} at which the overall electrostatic tip-surface is minimized before the

charging ($U_1^{'} = U_1$ - $U_{\mathrm{ini}} = (2.12 \pm 0.04)$ V and $U_2^{'} = U_2$ - $U_{\mathrm{ini}} = (3.98 \pm 0.04)$ V). For the ratio $n_2 \,/\, n_1$ we obtain a value of$\sim$1.9, which means that the NP contains two times more charges after the charging at peak 2 compared to the charging at peak 1.

3.4. FEM calculations

To get more insight into the charging, in particular with respect to the amount of transferred charges and the related strong changes in $\triangle f$ (figure 5a), we use the finite element method (FEM) and model the NP as a truncated sphere and the tip as a large cone ($h_{\mathrm{Cone}} = 1\,\mu$m, $\alpha_{\mathrm{Cone}} = 10^{\circ}$) with a spherical cap at its end (figure 5(b) and figure S6 and S7 in the supplementary material). Because the mean size of the features that are visible in the Kelvin image in figure 4(b) is around 30 nm, we model a blunt tip with a cap radius of $r_{\mathrm{Cap}} = 15$nm. Furthermore, because we suspect to have a nano-tip at the end of the tip (e.g., a NP), we attach a truncated small sphere at the spherical cap of the cone. Both, the NP and the nano-tip have a diameter of $2\,r_{\mathrm{NP}} = 2\,r_{\mathrm{Nanotip}} = 7.0$ nm, which matches the mean NP size obtained from constant height nc-AFM images (figure 1d). The dielectric film is modelled as a thin cylinder with a height and radius of $h_{\mathrm{Film}} = 40$ nm and $r_{\mathrm{Film}} = 1400$ nm, respectively, and has a dielectric constant of $\epsilon_{\mathrm{Film}} = 7$, which was measured for similar ALD grown Al_2O_3 films of same thickness [34]. Because a distance change of a few Ångströms leads to a tip-surface contact in the experiments (see above), we assume a distance of $z = 0.5$ nm between the top of the NP and the bottom of the nanotip. For the calculations of the detuning $\triangle f$, we use the experimental values $A = (15 \pm 5)$ nm, $f_0 = 70.88$ kHz and 2.4 N/m for the oscillation amplitude, cantilever resonance frequency and spring constant.

We mimic the charging by *explicitly* putting charges onto the main NP at the voltages of $U_{\mathrm{Peak1}} = +4.5$ and $U_{\mathrm{Peak2}} = +6.5$ V, which are the relative voltage positions of the two peaks with respect to the initial minimizing voltage ($U_{\mathrm{Peak1}} = U_{\mathrm{Peak}}^{'}$ - U_{ini}). As discussed above, we assume that two times more charges are put onto the NP at peak 2 compared to peak 1. Dirichlet conditions are used to apply a zero voltage at the tip and the bias voltage at the conducting support.

We first consider a single NP placed directly below the tip (figure 5(b)) and place 1 and 2 electrons onto the NP at U_{Peak1} and U_{Peak2}, respectively. The first curve (1) in figure 5(d) shows the corresponding $\triangle f(U_{\mathrm{Bias}})$ curve, which decreases down to -800 Hz at bias voltages of $\sim$+7.0 V. These large $\triangle f$ values do not considerably change if the size of the NP is changed by a few nanometres (figure S8c in the supplementary material). Furthermore, if a distance of $z = 1.0$ nm is chosen, the $\triangle f$ value increases onto -675 Hz but is still quite large (figure S9 in the supplementary material), and the same phenomena are observed which are described in the following.

At U_{Peak1} and U_{Peak2}, small peaks of $\sim$5 and $\sim$10 Hz, respectively, can be seen in $\triangle f$ (orange and red ellipses in inset of figure 5(d)). When increasing the amount of charges onto 5/10 electrons (curve 2) and 7/14 electrons (curve 3), the peaks increase in strength (curve 2: 66 / 87 Hz, curve 3: 92 / 114 Hz). However, they remain relatively small compared to the peaks observed in the experiment (231 and 176 HZ). Important to note is that the detuning $\triangle f$ values are still quite large at high bias voltages compared to the experimental values. This does not change if the tip-surface distance is increased onto, e.g., $z = 1.0$ nm (figure S9(b) in the supplementary material).

Overall, it can be concluded that due to the large $\triangle f$ values at high bias voltages and due to the small peak heights at U_{Peak1} and U_{Peak2}, the 'one NP setup' from above

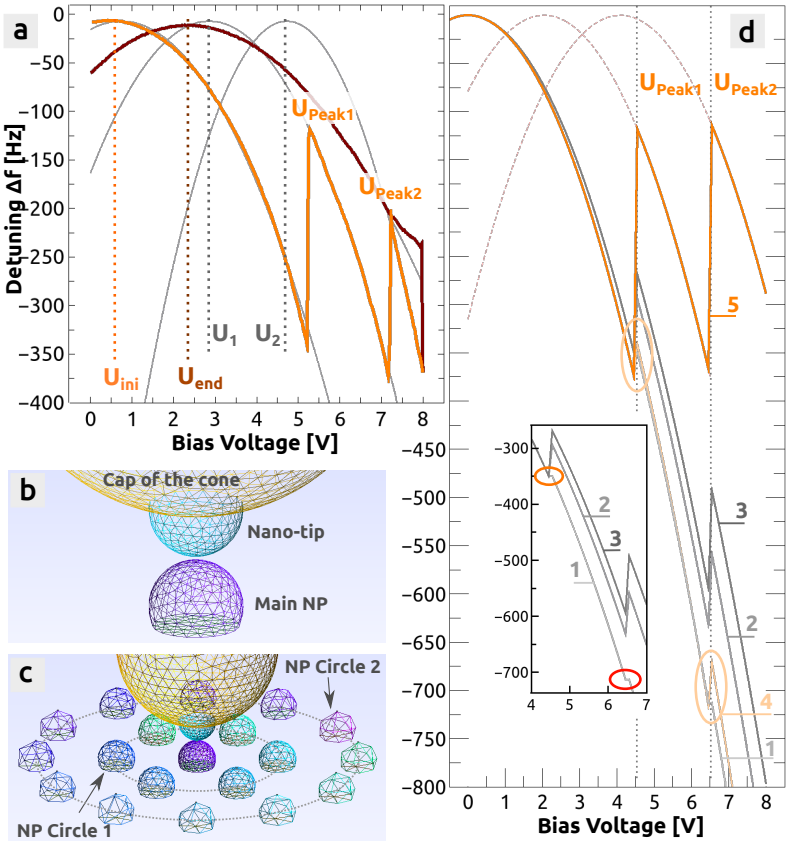

Figure 5. Comparison of experimental (a) and calculated (d) spectroscopic curves. The FEM models used for the simulations are shown in (b) and (c). (a) The experimental curves are the same as in figure 4(g). (b) In the FEM calculations, the nanotip is placed vertically above the NP that gets charged (main NP). (c) Eventually, 6 + 12 additional NPs can be placed around the main NP, evenly distributed on the two concentric circles 1 and 2. (d) At U_{Peak1} and U_{Peak2}, 1/2 (curve 1), 5/10 (curve 2) and 7/14 electrons (curve 3) are placed on the main NP without any nearby NPs, whereas 1/2 (curve 4) and 7/14 electrons (curve 5) are put onto the same main NP in the presence of all the other NPs (c).

does not describe our experimental observations. And indeed, when analysing the NP density around the charged NP (figure 4(a)) it is evident that rather an ensemble of NPs has to be considered: several NPs are located in close proximity to a NP, with a NP-NP distance between 15 and 18 nm. We therefore included several NPs into the model and arranged them in two circles with a radius of 15 and 30 nm around the main NP for simplicity (figure 5(c)). The inner and outer circle contain 6 and 12 nearby NPs, respectively, whereas the NPs on one circle are equidistant to each other. Although this arrangement does not represent the exact NP distribution in the experimental image, it is nevertheless representative from the NP density point of view: we slightly increased the NP density below the tip to compensate missing NPs, which would be otherwise distributed all over the surface as in the experiment.

When adding 1 and 2 electrons onto the main NP at U_{Peak1} and U_{Peak2},

respectively, the resulting $\triangle f(U_{\mathrm{Bias}})$ (curve 4) is quite similar to all the previous curves, with two peaks that have a height of 33 Hz (U_{Peak1}) and 46 Hz (U_{Peak2}). However, the curves change considerably when increasing the amount of charges onto 5/10 (Supplementary figure S10) and 7/14 electron charges (orange curve 5 in figure 5(d)): a peak height of 255 Hz and 251 Hz are found, respectively, which are comparable to the peak heights in the experiment (231 and 176 HZ). Due to these two high peaks, the detuning does not reach any more the very large values from the curves discussed before and is confined in a region of relatively small values below -400 Hz. The result is that, as in the experiment, two parabolic branches are visible after the two charging events. Fitting these two branches with $\triangle f(U_{\mathrm{Bias}}) = a\,(U_{\mathrm{Bias}} - U_{\mathrm{max}})^2$ yields two maxima at $U_{1,\mathrm{FEM}} = 2.04\,\mathrm{V}$ and $U_{2,\mathrm{FEM}} = 4.09\,\mathrm{V}$, which are comparable with the maxima from the experiment ($U_1^{'} = 2.12(4)\,\mathrm{V}$ and $U_2^{'} = 3.98(4)\,\mathrm{V}$).

To understand the strong increase of the peaks and the overall tip-surface interaction expressed by $\triangle f$, the electrostatic potential is analysed at the NPs. For the model with only the main NP and the one with the additional 18 nearby NPs, the two images in figure 6(a) and (b) show each a slice of the otherwise 3D electrostatic potential data at $U_{\mathrm{Bias}} = +8\mathrm{V}$ and with the main NP having 14 electron charges.

With respect to the single NP case (figure 6(a)), the main NP appears in one colour, which is due to the potential being constant all over the surface of the conducting but insulated NP. The same applies for all the nearby NPs. Although a single charged and isolated sphere of same size ($r = 3.5\,\mathrm{nm}$) with no nearby conductors is supposed to have a negative potential of $U = Q\,/\,C = \text{-}n\,e\,/\,(4\,\pi\,\varepsilon_0\,r) \approx \text{-}5.7\,\mathrm{V}$, the main NP here has a quite elevated positive potential of $+3.7\,\mathrm{V}$ (figure 6(c)), which is due to the presence of the tip and sample and in particular due to the relatively high bias voltage at the conducting support, in conjunction with the small film thickness ($h_{\mathrm{Film}} = 40\,\mathrm{nm}$) and the relative high dielectric constant of the film ($\epsilon_{\mathrm{Film}} = 7$). As shown in figure 6(c), the NP potential varies strongly in dependence on U_{Bias} and jumps upon the injection of electrons onto the NP whereas the number of electrons determines the strength of the jump.

Considering the 18 nearby NPs (figure 6(b)), the potential values of all these NPs are quite similar to the main NP potential at all U_{Bias} values (see figure 6(d)), which is due to the electrostatic induction effect: for a given system of conductors, a negative (positive) charge on only one conductor decreases (increases) the potential of all other insulated conductors [35]. As also shown in figure S10 and S11 in the supplementary material, the induction effect gets stronger when increasing the number of electrons on the main NP, the number of NPs around the main NP and when decreasing the radius of the two NP circles; in other words, the more and closer the NPs are the stronger is the electrostatic induction effect as expected.

With respect to the tip-surface interaction, the negative electrons inside the main NP have the tendency to tear the potential towards more negative potential values. The potentials of the 18 nearby NPs are adjusted accordingly so that the collective potential drop counteracts the strong interaction between the tip and conducting support. Secondly, a change of the NP's charge state gets amplified by the nearby NPs so that the peaks in $\triangle f(U_{\mathrm{Bias}})$ curves get larger. And furthermore, the $\triangle f(U_{\mathrm{Bias}})$ branches get displaced towards more positive voltage values.

Overall it can be concluded that only a collective potential drop of the main NP and the nearby NPs can explain the charging peaks in the experimental $\triangle f(U_{\mathrm{Bias}})$ curves of figure 4. Note that the number of transferred electrons inside the main NP may be slightly different due to the uncertainty of in particular the cantilever

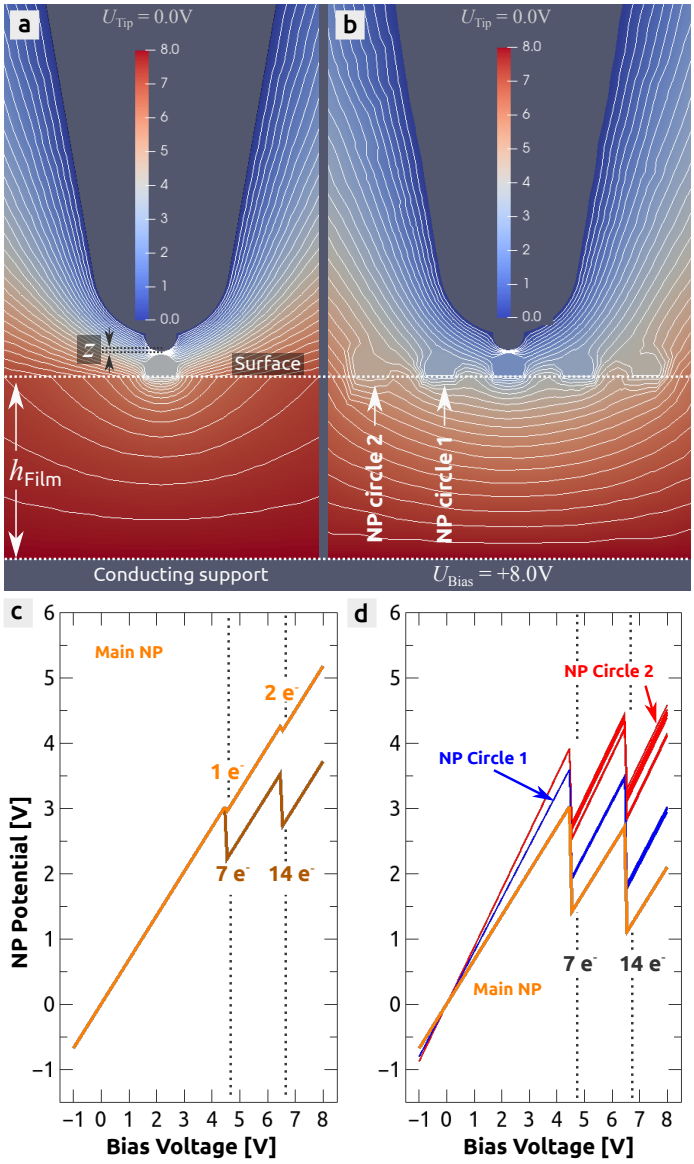

Figure 6. (a) and (b) The electrostatic potential represented in colour and by 30 equidistant potential lines (white) between the tip, NP, dielectric film and conducting support. The images show a concentric and perpendicular slice of the otherwise 3D potential data. (a) The model with only the main NP and with all 18 nearby NPs (b). (c) and (d) NP potential versus bias voltage curves for the 'one NP model' (c) and same model with the additional 18 nearby NPs (d).

oscillation amplitude, which has to be more precisely determined in future, e.g., in the same way as in Ref. [36]. Note that there is also some uncertainty in the NP size and tip-surface distance. We estimate an overall error of ∼40 % (∼3 electrons) for the number of transferred charges.

All the experimental observations and FEM calculations let assume that the

discrete charging events observed at the AuNPs are obviously due to an effect being similar to Coulomb blockades as observed before [7, 9, 11]. This is supported by the condition, which relates the charging energy given by $W_C = e^2 / 2\,C_{NP} \approx e^2 / 8\,\pi\,\varepsilon_0\,r_{NP}$ with the thermal energy of the system: $W_C \geq k_B\,T$. If we assume for simplicity a spherical NP with a size of $r_{NP} \approx 7\,\text{nm}$, we obtain $W_C \approx 0.206\,\text{eV} \approx 8\,k_B\,T$, with $T = 300\,\text{K}$ ($C_{NP} \approx 0.389\,\text{aF}$). Equally important signatures are certainly also the discrete charging events in the spectra, the 1:2 charge ratio and in particular the good agreement between experiment and theory.

Interestingly, it seems that the number of electrons transferred within one charging event is quite elevated (around 7 electrons) compared to the normal case of one electron only. This is a strong signature that the Al_2O_3 film cannot be considered as a perfect interface having no influence on the charging: because the alumina film is amorphous, there are potentially many sites on the surface and in subsurface regions underneath that can trap electrons, as we can indeed observe upon charging the film alone (figure S3 in the supplementary material) and by the possible tip-induced electron transfer from the NPs to the Al_2O_3 film (figure 2). And indeed, as reviewed recently [37], amorphous ZrO_2, HfO_2, SiO_2 and Al_2O_3 films are known to be acceptors for holes and electrons, whereas in particular electrons are the dominant charge carriers in ALD grown Al_2O_3 films, as shown by capacitance versus voltage (CV) experiments [22]. A theoretical study suspects in particular oxygen vacancies (V_O), aluminium (Al_i) and hydrogen interstitials (H_i), which can accept an electron [38].

Because the NP interface area is quite large ($\sim \pi\,r_{NP}^2 \approx = 3.8 \times 10^{-13}\,\text{cm}^2$, with $r_{NP} \approx 7\,\text{nm}$), several electrons can be possibly trapped at the interface and/or in the close subsurface region below. Considering the experiment shown in figure 5 with 7 electrons in one charging event, the electron density would be around $\sim 1.8 \times 10^{13}\,/\,\text{cm}^2$, which is ten times smaller than the value found in CV experiments [22] ($\sim 2 \times 10^{14}\,/\,\text{cm}^2$) and comparable with the value of $\sim 1 \times 10^{13}\,/\,\text{cm}^2$ of another work [23]. Note that due to the error of the number of injected electrons and of the NP size, our value of the electron density can vary by $\sim 40\,\%$ and more.

With respect to the charging mechanism, we assume that when the NP gets one electron, the electron is immediately trapped at the interface or subsurface region below and the NP can accept again an electron during the relatively slow sweeping of the bias voltage. The trapped electrons at the interface and in the NP are one charge source for the tip. The charging stops when the bias voltage passes the discrete charging voltage determined by the Coulomb blockade. However, we speculate that the maximum number of transferred electrons is not given by the sweep time over the charging voltage but rather by a saturation effect of surface/subsurface Al_2O_3 sites with electrons that is reached relatively quickly compared to the speed of the sweep.

4. Summary

We show that by using noncontact AFM (nc-AFM) spectroscopy and Kelvin probe force microscopy (KPFM) in UHV and at RT, a $\sim 5\,\text{nm}$ small AuNP on a 40 nm thick insulating Al_2O_3 film can be charged with a few electrons directly by the AFM tip. Controlled charge manipulation experiments can only be performed when the tip-surface distance is increased by some nanometers after the forward bias sweep, which avoids a possible back transfer of electrons from the NP to the tip during the backward bias sweep. Due to Coulomb blockades, characteristic charging peaks

can be seen in the forward $\triangle f(U_{\mathrm{Bias}})$ sweep, which appear at discrete and almost equidistant voltages in $\triangle f$. The peaks lead to a change of the otherwise parabolic $\triangle f(U_{\mathrm{Bias}})$ shape such that several parabolic branches are created, with maxima displaced towards more positive voltages. Finite element methode (FEM) calculations show that the electrostatic induction changes the potential of nearby AuNPs such that the overall surface potential gets strongly amplified when a charge is injected onto the main AuNP. This explains the experimentally observed large peaks in the $\triangle f(U_{\mathrm{Bias}})$ spectroscopy curves and the large voltage shifts of the parabolic $\triangle f(U_{\mathrm{Bias}})$ branches. The comparison with FEM reveals furthermore that a few electrons are transferred into the AuNP during one charge event. We anticipate that this might be due to a second transfer accompanied by an immediate trapping of the electrons into the Al_2O_3 film, either at the NP-Al_2O_3 interface or in close Al_2O_3 subsurface regions underneath the NP.

Our results motivate to conduct charge manipulation experiments also with other NPs and insulator supports. Thanks to the Coulomb blockades, transferred electrons can be counted, which helps for a detailed characterization of the charge interaction between the NP and the underlying support. The results on the electrostatic induction effect delivers the general message that any kind of surface device composed of closely arranged nano-objects is subject of strong surface potential modifications if the charge state of one nano-object is changed by a few electrons only. This is of particular importance in microelectronics where the mean dimension and next-neighbour distance of individual parts is in the lower nanometre range. With respect to heterogeneous catalysis, the adsorption and reaction of reactant and product molecules at NPs strongly depend on the NP charge and electrostatic potential, which motivates to study the catalytic activity of a single NP and NPs in close vicinity as a function of NP charge by nc-AFM and KPFM.

Acknowledgements

Support from the *Agence Nationale de la Recherche* (ANR) through project *CHAMAN* (grant ANR-17-CE24-0011) is gratefully acknowledged. We gratefully acknowledge stimulating discussions with D Martrou, Ph Rahe, R Olbrich and M Reichling.

References

[1] Barth C, Foster A S, Henry C R and Shluger A L 2011 *Adv. Mater.* **23** 477–501
[2] Zdrojek M, Mélin T, Boyaval C, Stiévenard D, Jouault B, Wozniak M, Huczko A, Gebicki W and Adamowicz L 2005 *Appl. Phys. Lett.* **86** 213114
[3] Hoff B, Henry C R and Barth C 2016 *Nanoscale* **8** 411–419
[4] Rahe P, Steele R P and Williams C C 2016 *Nano Lett.* **16** 911–916
[5] Roy-Gobeil A, Miyahara Y, Bevan K H and Grütter P 2019 *Nano Lett.* **19** 6104–6108
[6] Gross L, Mohn F, Liljeroth P, Repp J, Giessibl F J and Meyer G 2009 *Science* **324** 1428
[7] Stomp R, Miyahara Y, Schaer S, Sun Q, Guo H, Grütter P, Studenikin S, Poole P and Sachrajda A 2005 *Phys. Rev. Lett.* **94** 056802
[8] Azuma Y, Kanehara M, Teranishi T and Majima Y 2006 *Phys. Rev. Lett.* **96** 16108
[9] Cockins L, Miyahara Y, Bennett S D, Clerk A A, Studenikin S, Poole P, Sachrajda A and Grütter P 2010 *Proc. Natl. Acad. Sci.* **107** 9496–501
[10] Bennett S D, Cockins L, Miyahara Y, Grütter P and Clerk A A 2010 *Phys. Rev. Lett.* **104** 017203
[11] Tekiel A, Miyahara Y, Topple J M and Grütter P 2013 *ACS Nano* **7** 4683–4690
[12] Baris B, Alchaar M, Prasad J, Gauthier S, Dujardin E and Martrou D 2018 *Appl. Phys. Lett.* **112** 113101

[13] Goryl M, Krok F, Kolodziej J J, Piatkowski P, Such B and Szymonski M 2004 *Vacuum* **74** 223–227
[14] Barth C and Henry C R 2006 *Appl. Phys. Lett.* **89** 252119
[15] Sasahara A, Pang C L and Onishi H 2006 *J. Phys. Chem. B* **110** 13453–13457
[16] Glatzel T, Zimmerli L, Koch S, Kawai S and Meyer E 2009 *Appl. Phys. Lett.* **94** 063303
[17] Yurtsever A, Fernández-Torre D, Onoda J, Abe M, Morita S, Sugimoto Y and Pérez R 2017 *Nanoscale* **9** 5812–5821
[18] Khoussa H, Baris B, Alchaar M, Chaumeton F, Ghamnia M, Gauthier S and Martrou D 2018 *Phys. status solidi* **255** 1700482
[19] Grönbeck H and Barth C 2019 *J. Phys. Chem. C* **123** 4360–4370
[20] Dingemans G and Kessels W M M 2012 *J. Vac. Sci. Technol. A* **30** 040802
[21] Suh D 2021 *Phys. Status Solidi Rapid Res. Lett.* **2100236** 2100236
[22] Novikov Y N, Gritsenko V A and Nasyrov K A 2009 *Appl. Phys. Lett.* **94** 222904
[23] Li Y, Pei Y, Hu R, Chen Z, Ni Y, Lin J, Chen Y, Zhang X, Shen Z, Liang J, Fan B, Wang G and Duan H 2015 *IEEE Trans. Electron Devices* **62** 1184–1188
[24] Assaud L, Hanbücken M and Santinacci L 2013 *ECT Trans.* **50** 151–157
[25] Roy P, Badie C, Claude J B, Barulin A, Moreau A, Lumeau J, Abbarchi M, Santinacci L and Wenger J 2021 *ACS Appl. Nano Mater.* **4** 7199–7205
[26] Barth C, Claeys C and Henry C R 2005 *Rev. Sci. Instr.* **76** 083907
[27] Barth C, Hynninen T, Bieletzki M, Henry C R, Foster A S, Esch F and Heiz U 2010 *New J. Phys.* **12** 093024
[28] Hynninen T, Foster A S and Barth C 2011 *e-J. Surf. Sci. Nanotech.* **9** 6–14
[29] Alnæs M S, Blechta J, Hake J, Johansson A, Kehlet B, Logg A, Richardson C, Ring J, Rognes M E and Wells G N 2015 *Archive of Numerical Software* **3**
[30] Geuzaine C and Remacle J F 2020 *Int. J. Numer. Meth. Engng* 79
[31] Pakarinen O H, Barth C, Foster A S and Henry C R 2008 *J. Appl. Phys.* **103** 054313
[32] Barth C and Henry C R 2007 *Phys. Rev. Lett.* **98** 136804
[33] Schönenberger C and Alvarado S F 1990 *Phys. Rev. Lett.* **65** 3162–3164
[34] Groner M D, Elam J W, Fabreguette F H and George S M 2002 *Thin Solid Films* **413** 186–197
[35] Smythe W R 1989 *Static and Dynamic Electricity* 3rd ed (Taylor& Francis) ISBN 0-89116-917-2
[36] Heile D, Olbrich R, Reichling M and Rahe P 2021 *Phys. Rev. B* **103** 075409
[37] Strand J, Kaviani M, Gao D, El-Sayed A M, Afanas'ev V V and Shluger A L 2018 *J. Phys. Condens. Matter* **30** 233001
[38] Dicks O A, Cottom J, Shluger A L and Afanas'ev V V 2019 *Nanotechnology* **30** 205201